Onset of stationary and oscillatory convection in a tilted porous cavity saturated with a binary fluid: Linear stability analysis

Mohammad Karimi-Fard, Marie-Catherine Charrier-Mojtabi, Abdelkader Mojtabi

Onset of stationary and oscillatory convection in a tilted porous cavity saturated with a binary fluid: Linear stability analysis

M. Karimi-Fard, M. C. Charrier-Mojtabi, and A. Mojtabi
Institut de Mécanique des Fluides, U.M.R. 5502 CNRS-INP-UPS, Université Paul Sabatier, U.F.R. M.I.G. 118, route de Narbonne, 31062 Toulouse Cedex, France

In the present work, we study the onset of double-diffusive convective regimes in a tilted rectangular cavity, filled with a porous medium, saturated by a binary fluid. Two opposite walls are maintained at different but uniform temperatures and concentrations while the two other walls are impermeable and adiabatic. When the thermal and solutal buoyancy forces are comparable in intensity but have opposite signs, the motionless double-diffusive regime with linear temperature and concentration profiles is a solution of the problem. The first part of the study consists of a linear stability analysis of the motionless regime. We determine the critical thermal Rayleigh number for the onset of stationary and oscillatory convection. Indeed, we point out that there exist primary Hopf bifurcations for the studied problem in porous medium, while in the same configuration with a fluid medium only primary stationary bifurcations exist. When the first primary bifurcation creates a steady state branch of solutions, the bifurcation is either transcritical or pitchfork depending on the aspect ratio, A and the tilt, φ of the cavity. The onset of oscillatory convection (Hopf bifurcation) depends not only on A and φ but also on the Lewis number, Le and the normalized porosity, ϵ. Then, we determine the parts of the (Le, ϵ) parameter space for which the first primary bifurcation is stationary or oscillatory. In particular, it is found that in the case $\mathrm{Le} \geqslant 1$ and for $\epsilon\,\mathrm{Le}^2 < 1$ the first primary bifurcation is always a Hopf bifurcation for any A and φ except for $\varphi = +90°$. For $\epsilon\,\mathrm{Le}^2 > 1$ only stationary primary bifurcations exist. In the case $\mathrm{Le} < 1$, zones where stationary and oscillatory primary bifurcations exist are separated by a curve depending on A and φ. The last part of this work consists of a series of numerical simulations. The onset of stationary and oscillatory convection is obtained numerically at the critical Rayleigh number predicted by linear analysis. We also verified the frequency of oscillations for several sets of dimensionless parameters. The numerical simulations show multiple subcritical solutions.

I. INTRODUCTION

Natural convection in porous media is widely encountered in nature and technological processes. Water movement in geothermal reservoirs, underground spreading of chemical waste and other pollutants, grain storage, thermal insulation, evaporative cooling, and solidification are just a few examples where thermal natural convection or double-diffusive convection in porous media are observed.

The majority of the research effort has been devoted to the flow caused by a single buoyancy effect (thermal convection). Some of this literature has been reviewed by Combarnous and Bories[1] and Cheng.[2]

In some natural convection situations the heat transfer aspect cannot completly describe the phenomenon. Both heat and mass transfer must be considered. The presence of thermal and solutal buoyancy forces considerably modifies the flow within the porous media. The current state of knowledge concerning double-diffusive convection in a saturated porous medium is summarized in the studies developed by Trevisan and Bejan[3] and Nield and Bejan.[4] Of the many works in the literature related to double-diffusive convection in a cavity, the majority can be classified into two categories: cavities with imposed uniform heat and mass fluxes and cavities with imposed uniform temperature and concentration. It is important to note that most of these works are theoretical. We can mention three experimental studies in double-diffusive convection in porous media. The first was carried out by Griffith.[5] He observed a thin diffusive interface in a Hele–Shaw cell with salt and sugar or heat and salt as the diffusing components. He measured salt–sugar and heat–salt fluxes through two-layer convection systems and compared the results with predictions of a model. The second work was carried out by Imhoff and Green.[6] They studied double-diffusive groundwater fingers, using a sand-tank model and the salt–sugar system. They observed that double-diffusive groundwater fingers can transport solutes at rates as much as two orders of magnitude larger than those associated with molecular diffusion in motionless groundwater. This could play a major role in the vertical transport of near-surface pollutants in groundwater. The third experimental work, by Murray and Chen,[7] is closer to our study and concerns the onset of double-diffusive convection in a finite box filled with porous medium. The experiments were performed

in a horizontal layer consisting of 3-mm-diam glass beads contained in a box 24 cm×12 cm×4 cm high. The rigid top and bottom walls of the box provide a linear basic-state temperature profile but only allow a nonlinear time-dependent basic-state profile for salinity. They observed that when the porous medium is saturated with a fluid having a stabilizing salinity gradient, the onset of convection was marked by a dramatic increase in heat flux at the critical ΔT, and the convection pattern was three-dimensional, while two-dimensional rolls are observed for single-component convection in the same apparatus. They also observed a hysteresis loop on reducing the temperature difference from supercritical to subcritical values.

Concerning the theoretical studies, various modes of double-diffusive convection may exist depending on how both thermal and solutal gradients are imposed relative to each other and also on the numerous nondimensional parameters involved.

In the case of imposed uniform heat and mass fluxes, Trevisan and Bejan[8] considered a vertical porous cavity with imposed horizontal heat and mass fluxes. They developed an analytical Oseen-linearized solution for the boundary-layer regime for $\mathrm{Le}=1$, and proposed a similarity solution for heat-transfer-driven flows for $\mathrm{Le}>1$. These analytical results were validated by numerical experiments. The same configuration was studied by Alavyoon[9] and Alavyoon *et al.*[10] using numerical and analytical methods and scale analysis. They showed the existence of oscillatory convection in the case of opposing buoyancy forces. An extension of these studies to the case of the inclined porous layer subject to transverse gradients of heat and solute was carried out by Mamou *et al.*[11] They obtained an analytical solution by assuming parallel flow in the core region of the tilted cavity. The existence of multiple steady state solutions, for opposing buoyancy forces, has been demonstrated numerically. Mamou *et al.*[12] have also numerically shown that, in a square cavity where the thermal and solutal buoyancy forces counteract each other ($N=-1$), a purely diffusive (motionless) solution is possible even for Lewis numbers different from unity. For $\mathrm{Le}=10$ and $\mathrm{Ra}_T=100$ both the purely diffusive solution and convective states are possible.

The configuration of a horizontal porous layer, where the buoyancy effects are due to vertical or inclined gradients of temperature and concentration, was presented by Nield[13] and Nield *et al.*[14] They studied the onset of convection by linear stability analysis. The same configuration was considered later by Taunton *et al.*[15] and Trevisan and Bejan.[16] Taunton *et al.*[15] extended Nield's analysis and considered the salt-fingering convection case in a porous layer. Trevisan and Bejan[16] studied mass transfer in the case where the buoyancy effect is due entirely to temperature gradients. Rudraiah *et al.*[17] applied linear and nonlinear stability analysis and showed that subcritical instabilities are possible in the case of a two-component fluid. Brand *et al.*[18] obtained amplitude equations for the convective instability of a binary fluid mixture in a porous medium. They found an experimentally realizable example of a codimension-two bifurcation (intersections of stationary and oscillatory bifurcation lines).

The configuration of a vertical box with imposed temperature and concentration along the vertical sidewalls was considered by Trevisan and Bejan[19] and Charrier-Mojtabi *et al.*[20] Trevisan and Bejan[19] considered a square cavity submitted to horizontal temperature and concentration gradients. Numerical simulations are compared to a scaling analysis. They observed the development of a weak convection in the vicinity of $N=-1$ (N being the ratio of the solutal to the thermal buoyancy forces). They noticed that the flow disappears if the Lewis number, Le is equal to one and $N=-1$. Charrier-Mojtabi *et al.*[20] studied the linear stability of the purely diffusive regime, which exists for $N=-1$ and any Lewis numbers. They found that this solution is linearly stable up to a critical thermal Rayleigh number depending on the box aspect ratio and the Lewis number.

For the same boundary conditions, double-diffusive convection studies have been carried out in a fluid medium, for the case $N=-1$, by Gobin and Bennacer,[21] Ghorayeb and Mojtabi,[22] and Xin *et al.*[23] In all these stability analyses the first primary bifurcations lead to steady state solutions.

The purpose of this paper is a linear stability analysis of the purely diffusive solution, which exists when $N=-1$ in a tilted rectangular or infinite box filled with a porous medium saturated by a binary fluid. We complete the previous results obtained for an horizontal layer by Nield[13] and a vertical cavity by Charrier-Mojtabi *et al.*[20] The influence of the tilt of the cavity on the bifurcation points is analyzed. The most important part of this work concerns the study of the primary oscillatory instabilities which are only obtained in porous medium. In previous works these instabilities were studied only for the horizontal layer. Trevisan and Bejan[19] found, for the vertical box, that when $\mathrm{Le}=1$ and $N=-1$ the flow disappears completely. They did not consider unsteady flow. Charrier-Mojtabi *et al.*[20] assumed the principle of exchange of stability to be valid and concluded that the purely diffusive regime is infinitely linearly stable for $\mathrm{Le}=1$. Here, we carry out an extended linear stability analysis of this situation and we show the existence of oscillatory instability even for the case where $\mathrm{Le}=1$, and for various tilts of the cavity. Of course the case $N=-1$ would be difficult to obtain experimentally. However we believe that the study of this particular solution, which has not been completely described in previous works, will be useful for a better understanding of the more realistic situations $N=-1\pm\mu$, where μ is a small parameter.

II. MATHEMATICAL FORMULATION

We consider a tilted rectangular cavity of aspect ratio $A=H/L$ where H is the height of the cavity and L is the width. All the boundaries are impermeable. The cavity is filled with a porous medium and saturated by a Newtonian binary fluid. Figure 1 shows the geometry and the associated boundary conditions.

The cavity is assumed to be of infinite extent in the z direction. The superscript asterisks denote dimensional variables. The Oberbeck–Boussinesq approximation is applicable in the range of temperatures and concentrations expected. Thus, the fluid and porous material properties are

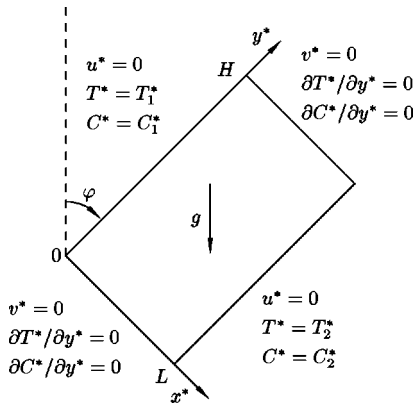

FIG. 1. Sketch of the problem.

constant, except the density of the fluid in the buoyancy contribution where it varies linearly with both local temperature and concentration

$$\rho=\rho_1[1-\beta_T(T^*-T_1^*)-\beta_C(C^*-C_1^*)],$$

where $\rho_1=\rho(T_1^*,C_1^*)$ is the reference density, $\beta_T=-(1/\rho_1)(\partial\rho/\partial T)_C$ and $\beta_C=-(1/\rho_1)(\partial\rho/\partial C)_T$ are the coefficients for thermal and solutal expansion. The fluid flow within the porous medium is assumed to be incompressible and governed by Darcy's law. We focus our study on the double-diffusive convection and so neglect the Soret and Dufour effects. The governing equations are

$$\nabla^*\cdot\mathbf{V}^*=0, \tag{1}$$

$$\left(\frac{\mu}{K}\right)\mathbf{V}^*=-\nabla^*P^*-\rho_f g\mathbf{k}^*, \tag{2}$$

$$\frac{(\rho c)_m}{(\rho c)_f}\frac{\partial T^*}{\partial t^*}+\mathbf{V}^*\cdot\nabla^*T^*=\alpha_m\nabla^{*2}T^*, \tag{3}$$

$$\epsilon'\frac{\partial C^*}{\partial t^*}+\mathbf{V}^*\cdot\nabla^*C^*=D_m\nabla^{*2}C^*, \tag{4}$$

where $\mathbf{V}^*=(u^*,v^*,w^*),P^*,T^*,C^*$, are the seepage (Darcy) velocity, pressure, temperature, and concentration, respectively. $\mathbf{k}^*=-\sin\varphi\mathbf{x}+\cos\varphi\mathbf{y}$ defines the tilt of the cavity and g the gravitational acceleration. The subscripts m and f refer to the porous medium and the fluid, respectively. The porous matrix is characterized by its permeability K and its porosity ϵ'. μ and c denote the viscosity of the fluid and the specific heat. α_m is defined as the effective thermal conductivity of the saturated porous medium divided by the specific heat capacity of the fluid. Parameter D_m represents the diffusivity of the constituent through the fluid-saturated porous matrix. The boundary conditions associated with Eqs. (1)–(4) are

$$\begin{aligned}&\mathbf{V}^*\cdot\mathbf{n}=0 \quad \text{at all boundaries},\\ &T^*=T_1^*,\ C^*=C_1^* \quad \text{at } x^*=0,\\ &T^*=T_2^*,\ C^*=C_2^* \quad \text{at } x^*=L,\\ &(\partial T^*/\partial y^*)=(\partial C^*/\partial y^*)=0 \quad \text{at } y^*=0 \text{ and } y^*=H.\end{aligned} \tag{5}$$

We define nondimensional quantities by

$$(x,y,z)=\mathbf{x}=\left(\frac{1}{L}\right)\mathbf{x}^*,\quad t=\left(\frac{\alpha_m(\rho c)_f}{L^2(\rho c)_m}\right)t^*,$$

$$(u,v,w)=\mathbf{V}=\left(\frac{L}{\alpha_m}\right)\mathbf{V}^*,$$

$$T=\frac{T^*-T_1^*}{T_2^*-T_1^*},\quad C=\frac{C^*-C_1^*}{C_2^*-C_1^*},$$

$$P=\frac{K(P^*+\rho_1 g(-\sin\varphi x^*+\cos\varphi y^*))}{\mu\alpha_m}.$$

The dimensionless governing equations now take the form

$$\nabla\cdot\mathbf{V}=0, \tag{6}$$

$$\mathbf{V}=-\nabla P+(\mathrm{Ra}_T T+\mathrm{Ra}_C C)\mathbf{k}, \tag{7}$$

$$\frac{\partial T}{\partial t}+\mathbf{V}\cdot\nabla T=\nabla^2 T, \tag{8}$$

$$\epsilon\frac{\partial C}{\partial t}+\mathbf{V}\cdot\nabla C=\frac{1}{\mathrm{Le}}\nabla^2 C, \tag{9}$$

$$\mathbf{k}=-\sin\varphi\mathbf{x}+\cos\varphi\mathbf{y},$$

where $\mathrm{Ra}_T=\rho_1 g\beta_T KL(T_2^*-T_1^*)/\mu\alpha_m$, $\mathrm{Ra}_C=\rho_1 g\beta_C KL(C_2^*-C_1^*)/\mu\alpha_m$ are the thermal and solutal Rayleigh numbers, respectively. $\epsilon=\epsilon'(\rho c)_f/(\rho c)_m$ is the normalized porosity and $\mathrm{Le}=\alpha_m/D_m$ the Lewis number.

The boundary conditions become

$$\begin{aligned}&\mathbf{V}\cdot\mathbf{n}=0 \quad \text{at all boundaries},\\ &T=C=0 \quad \text{at } x=0,\\ &T=C=1 \quad \text{at } x=1,\\ &(\partial T/\partial y)=(\partial C/\partial y)=0 \quad \text{at } y=0 \text{ and } y=A,\end{aligned} \tag{10}$$

where $A=H/L$ is the aspect ratio.

We are mainly interested in the special case where the thermal and solutal buoyancy forces are comparable in intensity but have opposite signs, so we have $\mathrm{Ra}_T=-\mathrm{Ra}_C$ or the buoyancy ratio $N=(\beta_C\Delta C^*)/(\beta_T\Delta T^*)=-1$. The number of dimensionless parameters is decreased and the Darcy equation becomes

$$\mathbf{V}=-\nabla P+\mathrm{Ra}_T(T-C)\mathbf{k}. \tag{11}$$

III. LINEAR STABILITY ANALYSIS

Motionless double-diffusive solution ($\mathbf{V}_0=0$, $T_0=x$, $C_0=x$) is a particular solution of the set of equations (6)–(10) and (11). To study the stability of this solution, we introduce infinitesimal three-dimensional perturbations $(\mathbf{v},\theta,c)$ defined by

$$\mathbf{v}=\mathbf{V}-\mathbf{V}_0,\quad \theta=T-T_0,\quad c=C-C_0,$$

where $\mathbf{V}$, T, and C indicate the disturbed quantities. The second-order smaller quantities are neglected. Due to the fact that the velocity field components are not coupled, a new system of three independent variables (u,θ,c) is considered,

where u is the component of the velocity field perturbation in the **x** direction. The linearized equations take the form

$$\nabla^2 u = -\mathrm{Ra}_T\left[\frac{\partial^2(\theta-c)}{\partial x\partial y}\cos\varphi + \left(\frac{\partial^2(\theta-c)}{\partial y^2}+\frac{\partial^2(\theta-c)}{\partial z^2}\right)\sin\varphi\right], \tag{12}$$

$$\nabla^2\theta = \frac{\partial\theta}{\partial t}+u, \tag{13}$$

$$\nabla^2 c = \mathrm{Le}\left(\epsilon\frac{\partial c}{\partial t}+u\right), \tag{14}$$

with the boundary conditions

$$u=\theta=c=0 \quad \text{at } x=0,1, \quad \forall y,\forall z,\forall t,$$
$$(\partial u/\partial y)=(\partial\theta/\partial y)=(\partial c/\partial y)=0 \quad \text{at } y=0,A, \ \forall x,\forall z,\forall t. \tag{15}$$

IV. ONSET OF STATIONARY CONVECTION

In this section we seek instability via stationary convection. The case of oscillatory convection is studied in Sec. V. From the steady state form of Eqs. (13) and (14) we deduce $\nabla^2(c/\mathrm{Le}-\theta)=0$. Because of boundary conditions (15) this last result leads to $c=\mathrm{Le}\,\theta$. Under this assumption the perturbation equations can be reduced to a new one with only the temperature perturbation

$$\nabla^4\theta = \mathrm{Ra}_T(\mathrm{Le}-1)\left[\frac{\partial^2\theta}{\partial x\partial y}\cos\varphi+\left(\frac{\partial^2\theta}{\partial y^2}+\frac{\partial^2\theta}{\partial z^2}\right)\sin\varphi\right]. \tag{16}$$

A. Case of an infinite layer

A cell of infinite extension in directions y and z is considered. The temperature perturbation is written as follows:

$$\theta=\theta(x)e^{I(ky+lz)},$$

where k and l are the wave number in directions y and z, respectively, and I is the imaginary unit. Perturbation equation (16) leads to

$$\theta^{(4)}-2(k^2+l^2)\theta''+(k^2+l^2)^2\theta = \mathrm{Ra}_T(\mathrm{Le}-1)[Ik\theta'\cos\varphi-(k^2+l^2)\theta\sin\varphi], \tag{17}$$

with boundary conditions

$$\theta=\theta''=0 \quad \text{at } x=0,1, \ \forall y,\forall z, \tag{18}$$

where $\theta''=d^2\theta/dx^2$.

1. Compound matrix method

Equation (17), and the associated boundary conditions (18), are solved using the compound matrix method. A very clear description of this method and its application to hydrodynamic stability problems is given by Drazin and Reid[24] and Straughan.[25] Here, we briefly show how this method is used to find the critical Rayleigh number corresponding to the lowest eigenvalue of (17). To solve problem (17) and (18) by the compound matrix method we let $\Theta=(\theta,\theta',\theta'',\theta''')^T$. To determine the lowest eigenvalue, we retain the two conditions at $x=0$ and the conditions at $x=1$ on θ and θ'' are replaced by $(\theta'(0)=1,\ \theta'''(0)=0)$ and $(\theta'(0)=0,\ \theta'''(0)=1)$. Thus, the boundary value problem is converted into an initial value problem. The solution can be written as a linear combination of Θ_1 and Θ_2 with initial condition $(0,1,0,0)^T$ and $(0,0,0,1)^T$,

$$\Theta=\alpha_1\Theta_1+\alpha_2\Theta_2$$

where α_1 and α_2 are constant. A new vector

$$Y=(y_1,y_2,y_3,y_4,y_5,y_6)^T,$$

is defined as the 2×2 minors of the 4×2 solution matrix whose first column is Θ_1 and second Θ_2. So,

$$\begin{aligned}
y_1&=\theta_1\theta_2'-\theta_1'\theta_2,\\
y_2&=\theta_1\theta_2''-\theta_1''\theta_2,\\
y_3&=\theta_1\theta_2'''-\theta_1'''\theta_2,\\
y_4&=\theta_1'\theta_2''-\theta_1''\theta_2',\\
y_5&=\theta_1'\theta_2'''-\theta_1'''\theta_2',\\
y_6&=\theta_1''\theta_2'''-\theta_1'''\theta_2''.
\end{aligned}$$

By direct calculation from (17) the initial value problem for Y is found to be $Y'=\mathcal{L}(Y)$ where $\mathcal{L}$ is a linear operator defined by

$$\begin{aligned}
y_1'&=y_2,\\
y_2'&=y_3+y_4,\\
y_3'&=I\,\mathrm{Ra}_T(\mathrm{Le}-1)k\cos\varphi y_1+2(k^2+l^2)y_2+y_5,\\
y_4'&=y_5,\\
y_5'&=[(k^2+l^2)^2+\mathrm{Ra}_T(\mathrm{Le}-1)\sin\varphi(k^2+l^2)]y_1\\
&\quad+2(k^2+l^2)y_4+y_6,\\
y_6'&=[(k^2+l^2)^2+\mathrm{Ra}_T(\mathrm{Le}-1)\sin\varphi(k^2+l^2)]y_2\\
&\quad-I\,\mathrm{Ra}_T(\mathrm{Le}-1)k\cos\varphi y_4.
\end{aligned} \tag{19}$$

The initial conditions for (19) are obtained from the initial conditions on Θ_1 and Θ_2,

$$Y(0)=(0,0,0,0,1,0)^T,$$

the boundary conditions on θ at $x=1$, $(\theta(1)=\theta''(1)=0)$, lead to the following condition:

$$y_2(1)=0. \tag{20}$$

Equation (19) is solved using a fourth-order Runge–Kutta algorithm. A shooting method is used to reach condition (20).

2. Numerical results

Figure 2 shows the critical nondimensional stability parameter $\mathrm{Ra}_{T_c}(\mathrm{Le}-1)$ as a function of φ for several values of wave number l. The associated wave number k (which is not plotted) corresponds to the critical value for which $\mathrm{Ra}_{T_c}(\mathrm{Le}-1)$ is minimum. It is found that the critical nondimensional

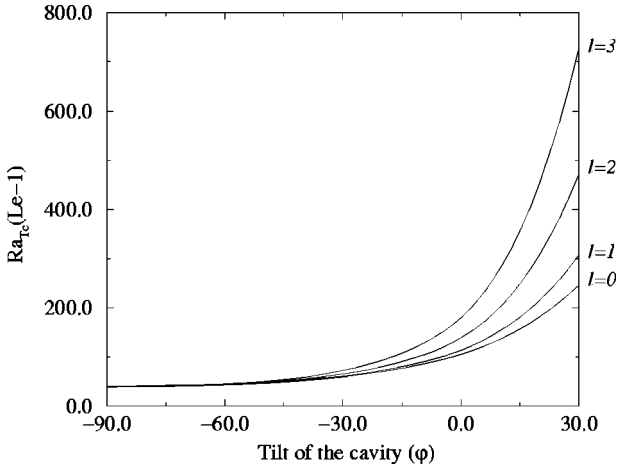

FIG. 2. Influence of three-dimensional perturbations on critical thermal Rayleigh number. Case of an infinite layer and for Le>1.

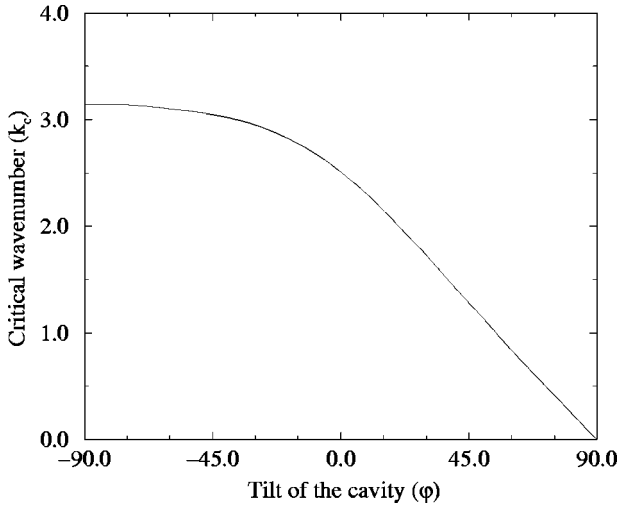

FIG. 4. Critical wave number k_c vs tilt φ for Le>1.

stability parameter $\mathrm{Ra}_{T_c}(\mathrm{Le}-1)$ is minimum for $l=0,\forall\varphi$. This latter result shows that the most dangerous perturbations in the case of an infinite layer are localized in the (*xoy*) plane. Figures 3 and 4 give the variations of the critical parameter $\mathrm{Ra}_{T_c}(\mathrm{Le}-1)$ and the critical wave number k_c with respect to the tilt of the layer. These results are obtained for Lewis numbers higher than one. In this case (Le>1), the thermal diffusivity is higher than the mass diffusivity which means that the concentration perturbations are predominant. Thus, the stability of the motionless solution depends directly on the destabilizing effects of the concentration. This behavior is brought out in Fig. 3. One can see that the lowest critical parameter is obtained for $\varphi=-90°$ (the upside wall is maintained at the highest concentration), which corresponds to the case where the concentration field is the most destabilizing. This destabilizing effect decreases with φ, which induces the increase of critical parameter. For Lewis number lower than one, the stability of the solution will depends on the destabilizing effects of the temperature. The above results hold with the following transformation:

$$\varphi\rightarrow-\varphi,$$

$$\mathrm{Ra}_T(\mathrm{Le}-1)\rightarrow\mathrm{Ra}_T(1-\mathrm{Le}).$$

In two extreme limits of φ, ($\varphi=\pm90°$) we have the stability problem analogous to Lapwood's one.[26] The thermal Rayleigh number of the Lapwood problem is replaced by $-\mathrm{Ra}_T(\mathrm{Le}-1)$. For $\varphi=-90°$ the motionless double-diffusive solution loses its stability for $\mathrm{Ra}_{T_c}=4\pi^2/(\mathrm{Le}-1)$ and the associated wave number is $k_c=\pi$. This previous result was first obtained by Nield.[13] For $\varphi=+90°$ the purely diffusive solution is infinitely linearly stable. For a tilted layer the motionless diffusive solution of the thermal problem is unstable. But, with a double-diffusive problem, the buoyancy force due to the solutal gradient can keep the motionless double-diffusive solution stable, even if the infinite layer is not horizontal. For the particular case of the vertical layer ($\varphi=0°$), Charrier-Mojtabi *et al.*[20] found $\mathrm{Ra}_{T_c}|\mathrm{Le}-1|=105.33$ and $k_c=2.51$. Table I summarizes the critical Rayleigh and wave number obtained for several tilts of the infinite layer.

Using the compound matrix method, the eigenvector associated to the eigenvalue $\mathrm{Ra}_{T_c}(\mathrm{Le}-1)$ is determined and used to calculate the streamfunction at the bifurcation point. Figure 5 shows the evolution of the convective flow pattern

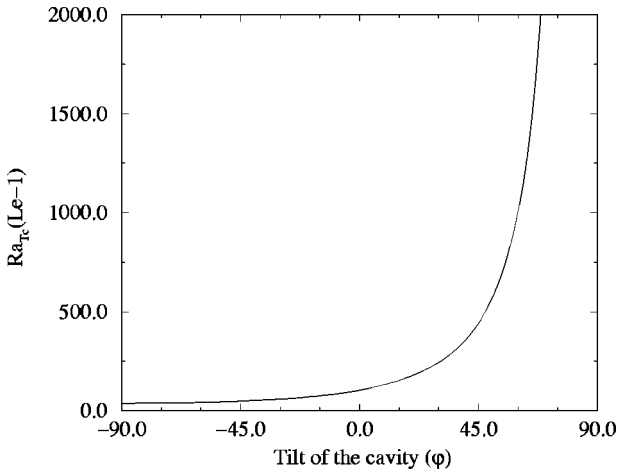

FIG. 3. $\mathrm{Ra}_{T_c}(\mathrm{Le}-1)$ vs tilt φ for Le>1.

TABLE I. Critical thermal Rayleigh number and the corresponding critical wave number for several tilts of the layer.

φ	$\mathrm{Ra}_{T_c}(\mathrm{Le}-1)$	k_c
−90°	39.478 ($4\pi^2$)	3.14 (π)
−75°	40.47	3.13
−60°	43.65	3.10
−45°	49.68	3.05
−30°	59.92	2.95
−15°	76.93	2.78
0°	105.33	2.51
+15°	154.31	2.15
+30°	245.43	1.73
+45°	442.15	1.28
+60°	1003.08	0.844
+90°	∞	0

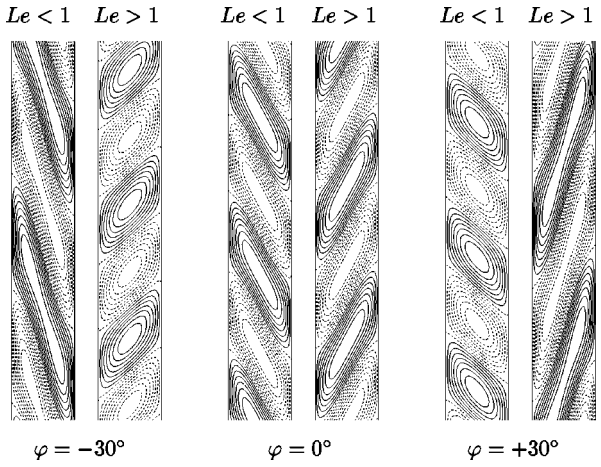

FIG. 5. Influence of the Lewis number Le and the tilt φ on the flow pattern at the bifurcation point.

at the bifurcation point for several tilts of the layer and for Lewis numbers, higher and lower than one. One can observe a succession of counter-rotating tilted cells. To understand qualitatively the tilt of the cells we consider the case Le <1. In this case the mass diffusivity is higher than the thermal diffusivity and the fluid needs more time to reach the surrounding temperature than the surrounding concentration. Accordingly, when we consider a fluid trajectory from the cold wall to the hot wall, the fluid particle on this trajectory is regularly in a hotter environment which deviate it downward. Likewise, there is an upward trajectory when the fluid particle moves from the hot wall to the cold wall. The same arguments explain the tilt of the cells in the case Le>1.

B. Case of a rectangular cavity

Now, only two-dimensional perturbations are considered. Equation (16) is solved using the Galerkin method with

$$\theta(x,y)=\sum_{n=1}^{N}\sum_{m=0}^{M} a_{nm}\sin(n\pi x)\cos\left(m\pi\frac{y}{A}\right).$$

Figure 6 presents the variations of $\mathrm{Ra}_{T_c}(\mathrm{Le}-1)$ for several aspect ratios A, as a function of the tilt φ. The curves are compared to the critical value of an infinite cell. The minimum value of the stability parameter is obtained for an infinite cell for any tested tilt. We can conclude that the confinement stabilizes the motionless double-diffusive solution. One can also notice that the situation of heating from the top, where the highest concentration is maintained, is the most unstable situation when the Lewis number is higher than one.

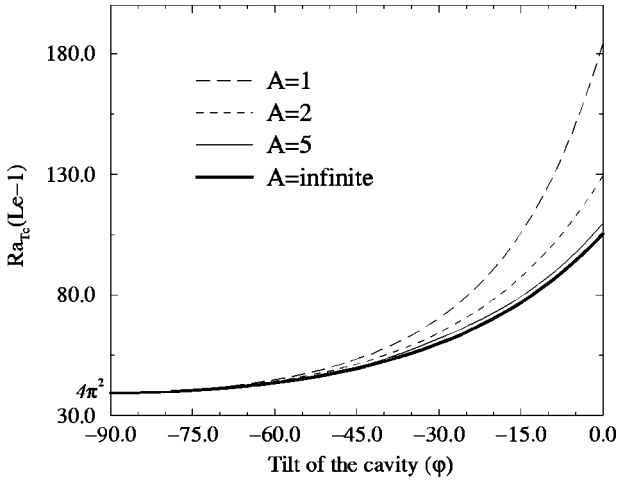

FIG. 6. Influence of the aspect ratio A and the tilt φ on $\mathrm{Ra}_{T_c}(\mathrm{Le}-1)$.

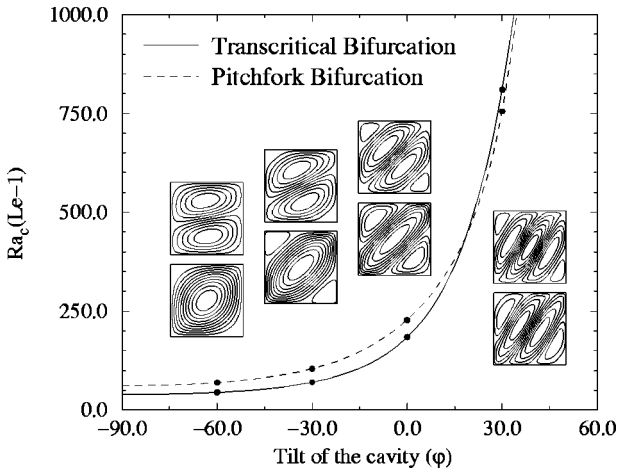

FIG. 7. Influence of the inclination on the type of the bifurcation for a square cavity. The evolution of streamfunction at the bifurcation points is presented for $\varphi=-60°$, $-30°$, 0°, and $+30°$. The streamfunctions associated with the first bifurcation are drawn at the bottom.

C. Transcritical and pitchfork bifurcation

The type of the bifurcations can be predicted by the symmetry properties of Eqs. (12)–(14) with boundary conditions (15). As a matter of fact in a rectangular cavity of aspect ratio A, the perturbation equations and the associated boundary conditions are invariant under combined x,y reflection and by the inversion of the velocity, temperature, and concentration perturbation fields. This symmetry property can be described with the operator $\mathcal{S}$:

$$\mathcal{S}\begin{pmatrix} u \\ \theta \\ c \end{pmatrix}(x,y)=\begin{pmatrix} -u \\ -\theta \\ -c \end{pmatrix}(1-x,A-y).$$

If (u,θ,c) is solution of (12)–(14), then $\mathcal{S}(u,\theta,c)$ is also solution of these equations. Thus Eqs. (12)–(15) possess centrosymmetry. The eigenvectors of the linear stability problem will be centrosymmetric with an odd number of cells or anticentrosymmetric with an even number of cells. The corresponding bifurcation is transcritical for centrosymmetric eigenvector and pitchfork for anticentrosymmetric eigenvector (Crawford and Knobloch[27]). In the present study, both transcritical and pitchfork bifurcations are obtained depending of the aspect ratio A and the tilt φ of the cavity. For a square cavity, the influence of the tilt of the cavity is presented in Fig. 7 and Table II. We can see the evolution of $\mathrm{Ra}_{T_c}(\mathrm{Le}-1)$ obtained for transcritical (solid line) and pitchfork (dashed line) bifurcations when the tilt φ increases. We also present the evolution of the streamfunction at the bifurcation points for different values of φ. The global behavior is

TABLE II. Critical thermal Rayleigh number corresponding to the transcritical and pitchfork bifurcations as a function of the tilt for $A=1$ (Galerkin method with $N=M=20$).

φ	Transcritical bifurcation $\mathrm{Ra}_{T_c}(\mathrm{Le}-1)$	Pitchfork bifurcation $\mathrm{Ra}_{T_c}(\mathrm{Le}-1)$
−90°	39.478 $(4\pi^2)$	61.69
−60°	44.92	69.66
−30°	70.36	104.75
0°	184.06	227.91
+30°	809.0	754.0

the same as for the infinite layer. The increase of the cavity tilt causes lengthening and the tilting of the cells.

Figure 8 shows the influence of the aspect ratio, A, on the bifurcation points for a vertical cavity ($\varphi=0°$). The two curves cross alternately at codimension two bifurcation points. When the aspect ratio increases, the flow patterns at the bifurcation points in the core region of the cavity lead to those observed for an infinite layer. We observe the same behavior for all tested tilts of the cavity (Fig. 9). One can notice a similar behavior for the same configuration in fluid medium (Gobin and Bennacer,[21] Ghorayeb and Mojtabi,[22] and Xin *et al.*[23]).

V. ONSET OF OSCILLATORY CONVECTION

In this section, the full equations (12)–(15) are considered. The term $e^{\sigma t}$ is introduced in the perturbation (u,θ,c) where σ is defined by $\sigma=\sigma_r+I\omega$ with I the imaginary unit. The perturbations are assumed to be two-dimensional and are developed as:

$$u(x,y,t)=\sum_{n=1}^{N}\sum_{m=0}^{M} a_{nm}\sin(n\pi x)\cos\left(m\pi\frac{y}{A}\right)e^{\sigma t}, \quad (21)$$

$$\theta(x,y,t)=\sum_{n=1}^{N}\sum_{m=0}^{M} b_{nm}\sin(n\pi x)\cos\left(m\pi\frac{y}{A}\right)e^{\sigma t}, \quad (22)$$

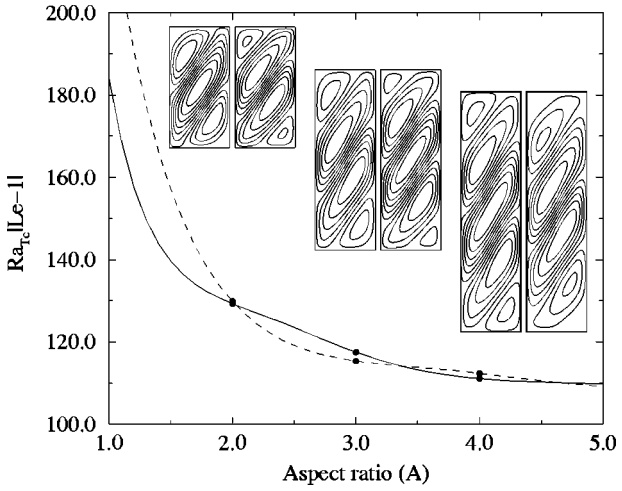

FIG. 8. Evolution of transcritical (the solid line) and pitchfork (the dashed line) bifurcations with respect to the aspect ratio for $\varphi=0°$. The streamfunctions associated with the first bifurcation are drawn on the left-hand side ($A=2$, 3, and 4).

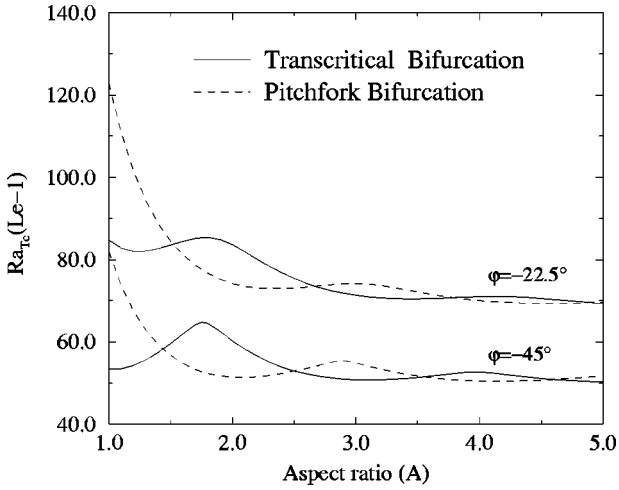

FIG. 9. Evolution of transcritical (the solid line) and pitchfork (the dashed line) bifurcations with respect to the aspect ratio for two slopes.

$$c(x,y,t)=\sum_{n=1}^{N}\sum_{m=0}^{M} c_{nm}\sin(n\pi x)\cos\left(m\pi\frac{y}{A}\right)e^{\sigma t}. \quad (23)$$

The marginal state corresponds to $\sigma_r=0$. The Galerkin method is used to solve the linear stability problem. We complete the previous results (transcritical and pitchfork bifurcations) by possible Hopf bifurcations. It is found that Hopf bifurcations exist and can appear before or after the transcritical or pitchfork bifurcations. The critical Rayleigh number for the Hopf bifurcation depends not only on the aspect ratio A, the tilt φ of the cell, and the Lewis number Le, but also on the normalized porosity ϵ. The overall study is difficult to carry out due to the numerous nondimensional parameters. The objective of this part is to identify the type of the first primary bifurcation (oscillatory or stationary bifurcation). We denote by stationary bifurcation all bifurcations toward stationary convection (transcritical or pitchfork). We first consider the two limit cases of horizontal cells ($\varphi=\pm 90°$). Then for general cases, we define the parts of the (Le, ϵ) parameter space for which the first primary bifurcation is stationary or oscillatory depending on the aspect ratio and the angle of tilt of the box.

A. Limit cases: $\varphi=\pm 90°$

In these situations the ''cross-derivative term'' in Eq. (12) is simplified. The problem can by solved by direct calculation and no numerical approximation is needed. Equations (12)–(14) become

$$\nabla^2 u=-\mathrm{Ra}_T J\left(\frac{\partial^2(\theta-c)}{\partial y^2}\right), \quad (24)$$

$$\nabla^2\theta=\frac{\partial\theta}{\partial t}+u, \quad (25)$$

$$\nabla^2 c=\mathrm{Le}\left(\epsilon\frac{\partial c}{\partial t}+u\right), \quad (26)$$

where J is defined by

$$\varphi = +90° \rightarrow J = +1,$$

$$\varphi = -90° \rightarrow J = -1.$$

The boundary conditions associated with this problem are

$$u = \theta = c = 0 \quad \text{at } x = 0,1, \ \forall y,$$
$$(\partial u/\partial y) = (\partial \theta/\partial y) = (\partial c/\partial y) = 0 \quad \text{at } y = 0,A, \ \forall x. \tag{27}$$

Solutions for (24)–(26) of the form (21)–(23) are possible if

$$B(B+\sigma)(B+\epsilon\sigma\,\mathrm{Le}) - \mathrm{Ra}_T CJ(B+\epsilon\sigma\,\mathrm{Le}) + \mathrm{Le}\,\mathrm{Ra}_T CJ(B+\sigma) = 0, \tag{28}$$

where

$$B = (i\pi)^2 + (j\pi/A)^2, \quad C = (j\pi/A)^2.$$

At marginal stability, $\sigma = I\omega$ where ω is real. The real and imaginary parts of Eq. (28) become

$$\mathrm{Ra}_T CJ(\mathrm{Le}-1) + (B^2 - \epsilon\omega^2\,\mathrm{Le}) = 0,$$

$$\omega(\mathrm{Ra}_T CJ\,\mathrm{Le}(1-\epsilon) + B^2(1+\epsilon\,\mathrm{Le})) = 0.$$

Two solutions are possible:

$$\omega = 0,$$
$$\mathrm{Ra}_T = J\left(\frac{B^2}{C}\right)\frac{1}{(1-\mathrm{Le})} \tag{29}$$

and

$$\omega^2 = \frac{B^2}{\epsilon\,\mathrm{Le}^2}\,\frac{(1-\epsilon\,\mathrm{Le}^2)}{(1-\epsilon)},$$
$$\mathrm{Ra}_T = J\left(\frac{B^2}{C}\right)\frac{(\epsilon+1/\mathrm{Le})}{(\epsilon-1)}. \tag{30}$$

1. Case: $\varphi = +90°$

The saturated porous medium is heated from below where the highest concentration is imposed. For Lewis numbers higher than or equal to one the motionless double-diffusive solution is infinitely linearly stable, $\forall\epsilon$. For Lewis numbers lower than one, the motionless solution loses its stability via a stationary bifurcation with $\mathrm{Ra}_{T_c} = \gamma_r/(1-\mathrm{Le})$. γ_r can be obtained by direct calculation from

$$\gamma_r = \min_{i,j}\frac{B^2}{C} = \min_{i,j}\frac{\left((i\pi)^2 + \left(\frac{j\pi}{A}\right)^2\right)^2}{\left(\frac{j\pi}{A}\right)^2}.$$

Figure 10 plots γ_r versus the aspect ratio A. The limit value of γ_r when $A \rightarrow \infty$ is equal to $4\pi^2$. Thus, for an infinite layer and $\mathrm{Le} < 1$ the results are identical to those obtained for the Lapwood problem.

2. Case: $\varphi = -90°$

The saturated porous medium is now heated from the top where the highest concentration is imposed. In this case, and for Lewis numbers higher than one, both stationary and Hopf bifurcations are possible. The direct calculation [Eqs. (29) and (30)] gives, for the stationary bifurcation, $\mathrm{Ra}_{T_c} = \gamma_r/(\mathrm{Le}-1)$ and the Hopf bifurcation is defined by

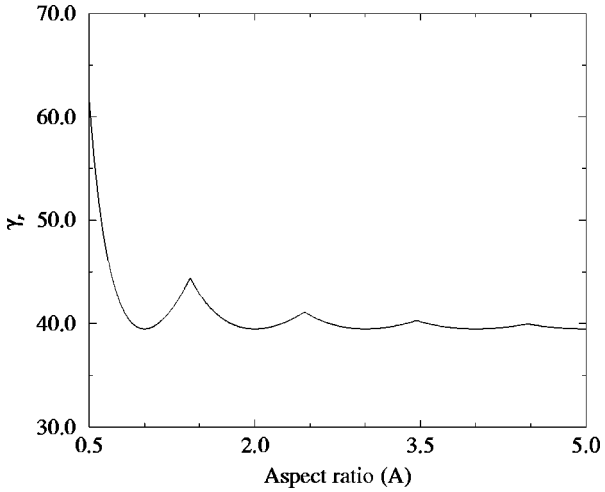

FIG. 10. γ_r vs aspect ratio.

$$\mathrm{Ra}_{T_c} = \gamma_r\frac{(\epsilon+1/\mathrm{Le})}{(1-\epsilon)}, \quad \omega_c^2 = \frac{\gamma_\omega}{\epsilon\,\mathrm{Le}^2}\,\frac{(1-\epsilon\,\mathrm{Le}^2)}{(1-\epsilon)}, \tag{31}$$

where γ_ω is defined by $\gamma_\omega = B^2 = ((i\pi)^2 + (j\pi/A)^2)^2$, where i and j have the same values as those determined for γ_r. Figure 11 reports γ_ω with respect to the aspect ratio. The limit value of γ_ω for an infinite horizontal layer is equal to $4\pi^4$. One can observe that γ_ω (consequently ω_c) is discontinuous for some aspect ratios. This means that for these critical aspect ratios there are two Hopf bifurcations at the same critical Rayleigh number, but with different critical pulsations. This is a codimension-two bifurcation point. The Hopf bifurcation defined by (31) exists only for $\epsilon\,\mathrm{Le}^2 < 1$, this condition guarantees that $\omega_c > 0$. For $\mathrm{Le} > 1$, this condition also guarantees the following relationship:

$$\frac{\epsilon+1/\mathrm{Le}}{1-\epsilon} < \frac{1}{\mathrm{Le}-1},$$

which means that in this situation the Hopf bifurcation appears before the stationary bifurcation. For Lewis numbers

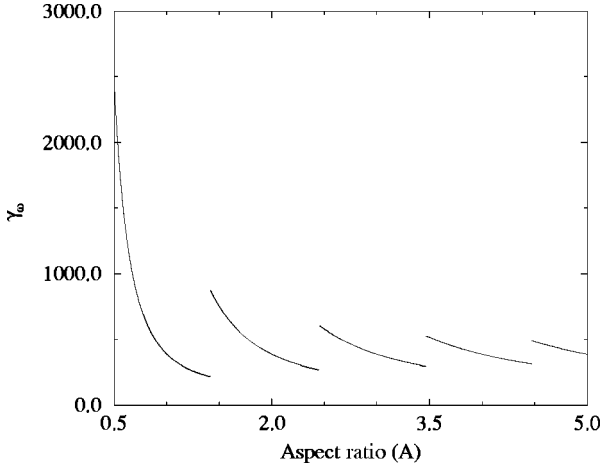

FIG. 11. γ_ω vs aspect ratio.

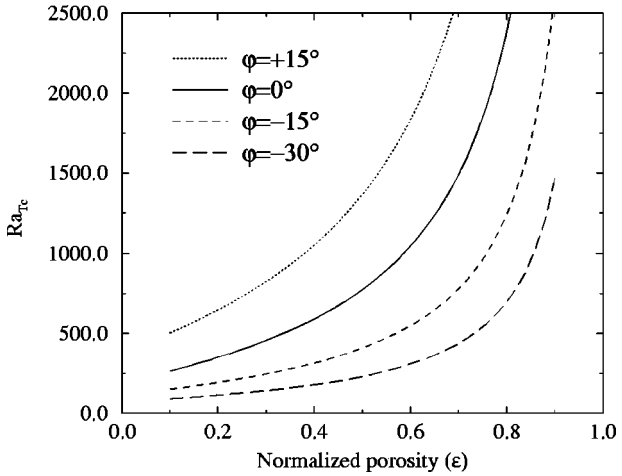

FIG. 12. Influence of the normalized porosity ϵ on the critical Rayleigh number Ra_{T_c} of the Hopf bifurcation for $A=1$ and $\mathrm{Le}=1$.

lower than or equal to one only Hopf bifurcations exist, $\forall \epsilon$. These results are corroborated by numerical simulations presented in Sec. VI.

B. General cases

In general cases (for any aspect ratio and for any tilt) the analytical resolution of the stability problem is not possible. We use a numerical approach based on the Galerkin method to solve the problem. Three situations are considered, $\mathrm{Le}=1$, $\mathrm{Le}>1$, and $\mathrm{Le}<1$.

1. Case: Le=1

The results obtained in Sec. IV show that for the Lewis number equal to one, the motionless double-diffusive solution is infinitely linearly stable. This result is obtained when only the stationary bifurcations are considered. A more complete analysis of this situation shows that the motionless solution can lose its stability via a Hopf bifurcation for $\mathrm{Le}=1$. Figures 12 and 13 show the influence of the normalized porosity on the critical Rayleigh number and the pulsation corresponding to the Hopf bifurcation in the case of a square cavity and for $\mathrm{Le}=1$. We can see that the critical Rayleigh number increases when the normalized porosity increases. This means that ϵ has a stabilizing effect. In this case, the mass and thermal diffusion coefficients are identical and they do not cause the instability. The cause of instability is the difference between the unsteady temperature and concentration profiles. This difference increases when ϵ decreases which is consistent with the results presented in Fig. 12. Moreover, for $\epsilon=1$, the temperature and concentration profiles are identical and there are not any sources of instability. The motionless double-diffusive solution is infinitely linearly stable.

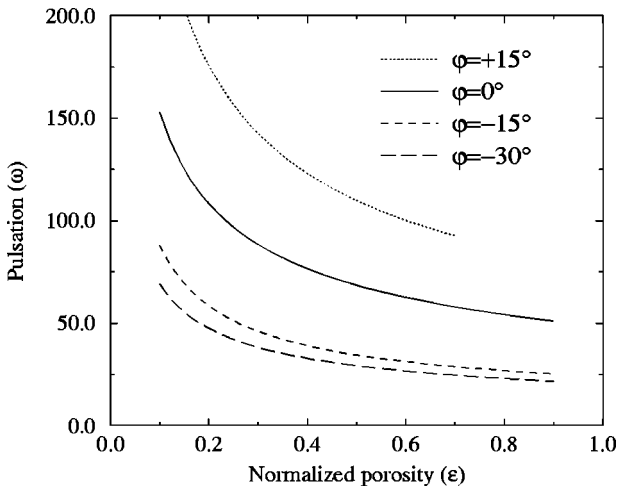

FIG. 13. Influence of the normalized porosity ϵ on the pulsation ω_c for $A=1$ and $\mathrm{Le}=1$.

2. Case: Le>1

For Lewis numbers higher than one, the numerical resolution of the perturbation equations shows the existence of two zones in the (Le, ϵ) parameter space separated by the curve $\epsilon\,\mathrm{Le}^2=1$. When $\epsilon\,\mathrm{Le}^2>1$, the first primary bifurcation creates steady state branches of solution and for $\epsilon\,\mathrm{Le}^2<1$, the first bifurcation is a Hopf bifurcation. It is important to observe that these results do not depend on either the aspect ratio or the tilt of the cavity. As can be observed in Fig. 14, the same curve was obtained for all tested angles of tilt.

3. Case: Le<1

For Lewis numbers smaller than one, the situation is more complicated. There are still two zones in the (Le, ϵ) parameter space, but they are separated by a curve depending on both the angle of tilt and the aspect ratio. Figure 14 shows the results obtained for a square cavity and for several angles of tilt. For each tested tilt, the zone where the first primary bifurcation is a stationary bifurcation and the zone where the first bifurcation is a Hopf one are separated by a curve of codimension-two bifurcation points. A section of Fig. 14 for $\epsilon=0.5$ is presented in Fig. 15. Figure 15 shows the evolution of critical Rayleigh numbers associated with transcritical and Hopf bifurcation as a function of Lewis number for $A=1$ and $\varphi=0°$. The curve of Hopf bifurcation crosses the transcritical curve at two codimension-two bifurcation points. For Lewis numbers lower than one the intersection point depends on all nondimensional parameters (A, φ, Le, and ϵ). On the contrary, for Lewis numbers higher than one, the intersection point is defined only by $\epsilon\,\mathrm{Le}^2=1$, the aspect ratio A and the tilt of the cell φ do not influence this point. Table III summarizes the values of the critical parameters obtained in the case ($A=1$, $\varphi=0°$, and $\epsilon=0.5$).

One can notice that for the problem of double-diffusive convection in fluid, in the same configuration the first bifurcation is never a Hopf one. The existence of Hopf bifurcation in porous medium may be explained through the normalized porosity. This parameter induces different evolution in time between the temperature and the concentration. This difference is enhanced when the normalized porosity decreases. Indeed, diffusion and advection of concentration can only be carried out in the space occupied by fluid, thus both diffusion and advection are magnified by ϵ^{-1} compared to diffusion and advection of heat.

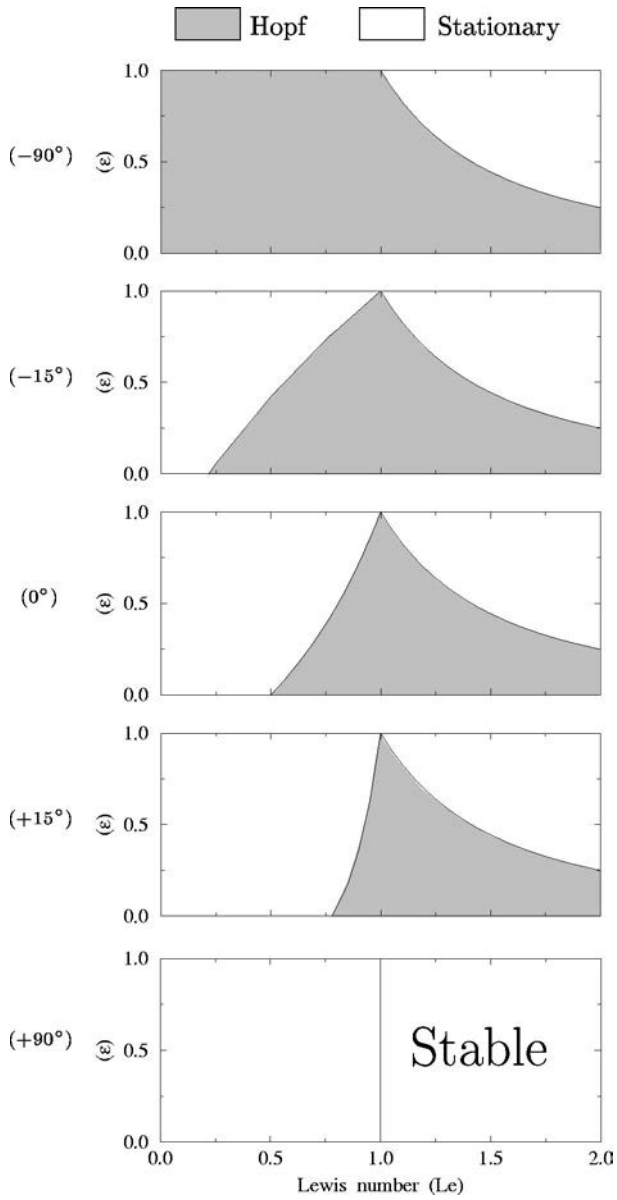

FIG. 14. Domains of the existence of stationary and Hopf bifurcations in (Le, ϵ) parameter space for $A=1$. For $\varphi=+90°$ and Le>1 the motionless solution is infinitely linearly stable.

VI. NUMERICAL SIMULATIONS

The governing equations (6)–(10) have been solved by a finite volume method that employs primitive variables on a staggered mesh (Patankar[28]). Diffusive and convective fluxes are discretized by central differencing. Solutions are obtained by fully implicit marching in time. The typical time step is 10^{-2}, but for oscillatory convection with high frequency, lower time steps are used (10^{-3}, 10^{-4}). The grid employed is uniform and consists of 41×41 volumes for a square cavity. The code was validated by comparing our results to those obtained by Goyeau *et al.*[29] and Trevisan and Bejan.[19]

To corroborate the results obtained with the linear stability analysis several numerical simulations were carried out. These simulations permit us to observe the onset of convection at the critical Rayleigh number predicted by the linear theory. In the case of oscillating convection, the frequencies obtained numerically are compared successfully with those obtained by linear stability analysis. Moreover, the time integration of the full set of nonlinear equations provides more information about the solution just after the bifurcation points. In particular, we get information about the stability of these solutions and the sense of rotation of the cells. We first consider the onset of stationary convection, then the results for oscillating convection are presented.

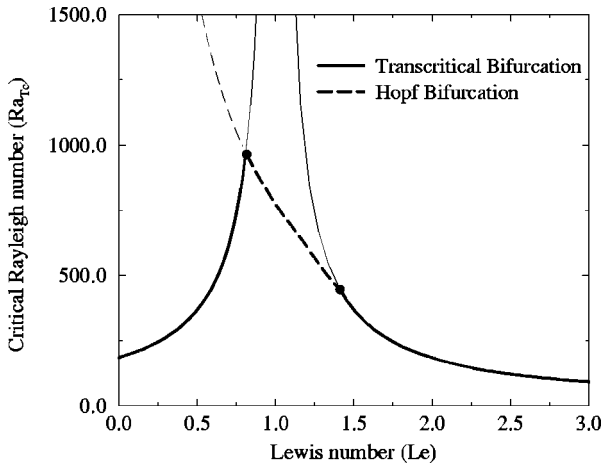

FIG. 15. Critical Rayleigh number vs Lewis number, for $A=1$, $\varphi=0$, and $\epsilon=0.5$.

A. Stationary convection

Numerical simulations are carried out for a square cavity ($A=1$) with Le$=2$. The normalized porosity ϵ, is kept equal to one, to avoid any primary Hopf bifurcation. The results are presented for four tilts of the cavity ($\varphi=-90°$, $\varphi=-60°$, $\varphi=-30°$, and $\varphi=0°$). As seen in Fig. 7 and Table II, for this set of parameters the purely diffusive regime loses stability via a transcritical bifurcation. The supercritical branch of solutions created at the bifurcation point is stable. The numerical values of the critical parameter $\mathrm{Ra}_{T_c}(\mathrm{Le}-1)$ are in very good agreement with those obtained by linear stability analysis. In Fig. 16, we report the supercritical convective solution pattern, close to the onset of convection, for a Rayleigh number slightly higher than the critical value. One can see that the streamlines obtained numerically by direct simulation are identical to the eigenvectors presented in Fig. 7. The numerical simulations show that the main center cell has a clockwise rotation. The two small counter-rotating cells located in the upper left-hand

TABLE III. Critical thermal Rayleigh number for the stationary and Hopf bifurcations for several Lewis numbers, for $A=1$, $\varphi=0°$, and $\epsilon=0.5$ using the Galerkin method with $N=M=15$. ($\times$) means the Hopf bifurcation does not exist.

Le	Ra_{T_c} (stationary)	Ra_{T_c} (Hopf)	ω_c
0.5	368.12	1591.	259.3
1.0	∞	818.	89.6
$\sqrt{2}$	444.36	444.36	0
2.0	184.06	$\times$	$\times$

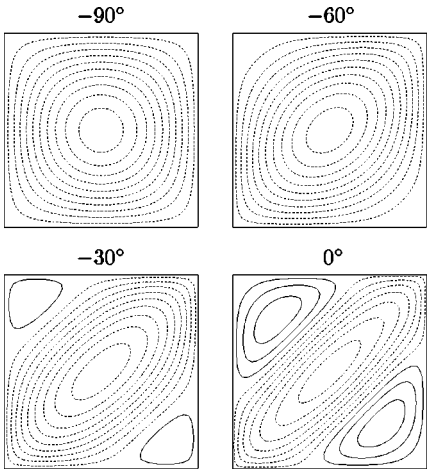

FIG. 16. Supercritical solution for $A=1$, Le$=2$, and for $\varphi=-90°,-60°,-30°,0°$. The Rayleigh numbers associated with each solution are slightly higher than the critical values.

and the lower right-hand corners of the box gradually disappear as φ decreases from 0° to −90°. At $\varphi=-90°$ the flow is similar to that obtained in a square cavity heated from below. The isotherms and isoconcentrations are not presented, but show a practically conductive state. For $\varphi=+30°$, the time integration of the nonlinear equations shows that the motionless double-diffusive solution loses its stability at the predicted critical Rayleigh number. Numerical simulation is carried out for $\mathrm{Ra}_T=760$. The time evolution of the v component velocity is plotted in Fig. 17. The flow pattern obtained before and after the transition is also presented. Before the transition, the flow pattern corresponds to the solution predicted by the linear analysis (Fig. 7) while after, the streamlines are completly different. Figure 18 represents the associated isotherms and isoconcentrations. They are highly deformed due to high velocity. This latter solution is a subcritical solution and does not correspond to the expected solution at the onset of convection. This would mean that the branch of solution issued from the pitchfork bifurcation is unstable. The convective solution persists when the Rayleigh number decreases, even for Rayleigh numbers lower than the critical value.

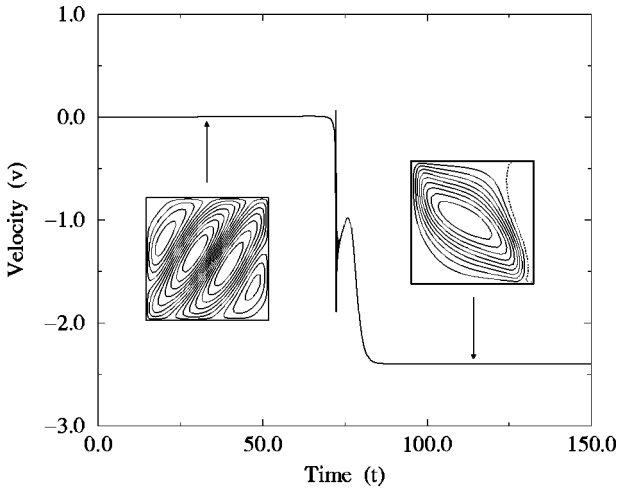

FIG. 17. The evolution in time of the velocity at the onset of convection for $A=1$, Le$=2$, $\varphi=+30°$, and $\mathrm{Ra}_T=760$.

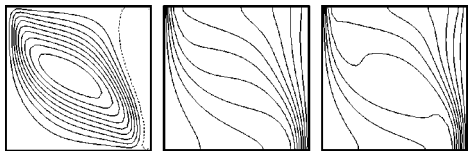

FIG. 18. Streamlines, isotherms, and isoconcentrations for $A=1$, Le$=2$, $\varphi=+30°$, and $\mathrm{Ra}_T=760$. Solid lines in streamlines correspond to counterclockwise rotations.

The complete study of the subcritical solutions is not the subject of the paper. Our numerical simulations show multiple subcritical and supercritical solutions. To describe these flows we must develop a continuation method. For the present work, to illustrate this multiplicity of solutions we have plotted the streamlines, the isotherms, and the isoconcentrations for different solutions obtained in the case $A=1$, Le$=2$, and $\mathrm{Ra}_T=195$ (Fig. 19). Solution (a) corresponds to the supercritical solution just after the onset of convection. The corresponding isotherms and isoconcentrations are slightly deformed due to low velocity. On the other hand, isotherms and isoconcentrations associated with solutions (b) and (c) are highly deformed. These solutions are part of two subcritical branches of solutions issued from a secondary pitchfork bifurcation.

B. Oscillatory convection

When the first primary bifurcation is a Hopf one, the results of the linear stability analysis are compared with numerical simulation for several situations. For the cavity heated from the top, where the highest concentration is imposed ($\varphi=-90°$), we consider a square cavity ($A=1$) filled with a porous medium characterized by $\epsilon=0.2$ and a binary fluid with Le$=2$.

With these parameters, the first primary bifurcation is a Hopf one with $\mathrm{Ra}_{T_c}=3.5\pi^2\simeq 34.54$ and $\omega_c^2=1.25\pi^4$ [obtained analytically from (31)]. The corresponding critical frequency is $f_c=\omega_c/2\pi\simeq 1.756$. The numerical simulation of

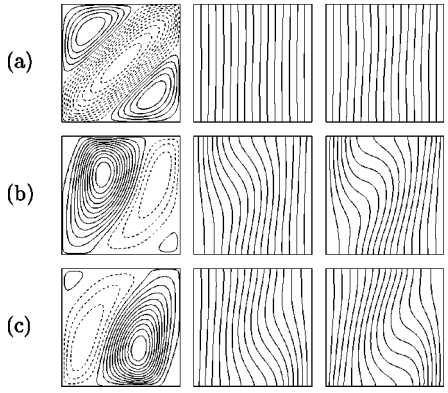

FIG. 19. Streamlines, isotherms, and isoconcentrations for $A=1$, Le$=2$, $\varphi=0°$, and $\mathrm{Ra}_T=195$. Solid lines in streamlines correspond to counterclockwise rotations. (a) Supercritical solution, (b) and (c) solutions on subcritical branches.

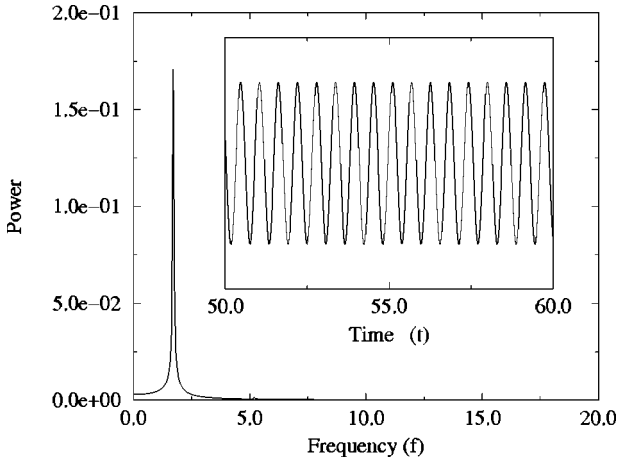

FIG. 20. Numerical determination of critical frequency of the Hopf bifurcation for $A=1$, Le$=2$, $\epsilon=0.2$, and $\varphi=-90°$.

this situation shows the existence of a stable branch of oscillatory solution just after the predicted critical Rayleigh number (Fig. 20). The frequency of the oscillations obtained for $\mathrm{Ra}_T=35$ is $f_{\mathrm{num}}\simeq 1.77$, which is in good agreement with the analytical results. The structure of the convective flow is a single rotating cell (identical to that obtained for stationary convection), but the sense of rotation changes periodically in time.

However, for most of the angles of tilt considered, the branch of solutions issued from the Hopf bifurcation is unstable. For several sets of values (A, φ, Le, and ϵ) the results of the linear stability analysis are validated by computing the frequency of the vanishing oscillations that occur when a perturbation is induced for a Rayleigh number slightly lower than the critical Rayleigh number predicted by the linear theory.

Figure 21 illustrates the case $A=1$, Le$=2$, $\epsilon=0.2$, and $\varphi=0°$ for which the linear stability predicts a Hopf bifurcation at $\mathrm{Ra}_{T_c}\simeq 170.7$ and $f_c=\omega_c/2\pi\simeq 2.24$. The numerical simulation gives, for a perturbation generated at $\mathrm{Ra}_T=169$, a

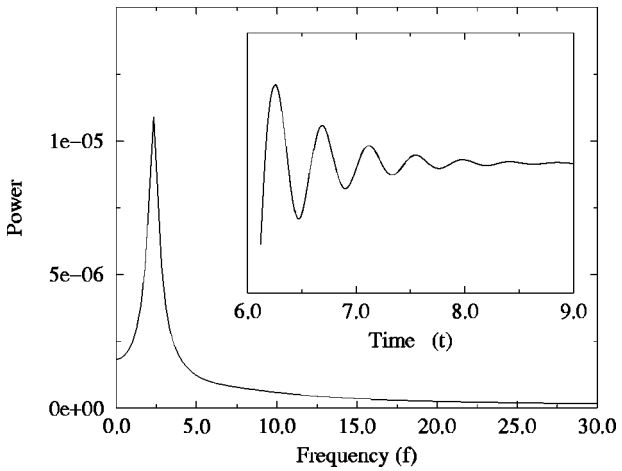

FIG. 21. Numerical determination of critical frequency of the Hopf bifurcation for $A=1$, Le$=2$, $\epsilon=0.2$, and $\varphi=0°$.

vanishing oscillation with the frequency $f_{\mathrm{num}}\simeq 2.3$, which is in good agreement with the results of the linear theory.

VII. CONCLUSION

An analytical and numerical study of the onset of double-diffusive convection in a tilted rectangular or infinite box, filled with a porous medium and saturated by a binary fluid, is carried out. In the case of an infinite layer tridimensional perturbations are considered and we show that bidimensional perturbations are the most dangerous. The first primary bifurcation creates either branches of steady solutions or time-dependent solutions via Hopf bifurcation. The type of bifurcation depends on the aspect ratio A, the tilt of the box φ, the Lewis number Le, and the normalized porosity ϵ. For the same problem in fluid medium the first primary bifurcation is never a Hopf bifurcation.

It is important to note that for most physical situations, the Lewis number is higher than one. Then, the present study shows that the type of the first primary bifurcation (stationary or oscillatory) depends only on Le and ϵ. The aspect ratio A and the tilt φ have an influence on the value of the critical parameters and the type of the stationary bifurcation (transcritical or pitchfork). The curve $\epsilon\,\mathrm{Le}^2=1$ in the (Le, ϵ) parameter space represents a set of codimension-two bifurcation points which separates the region where the first primary bifurcation is a Hopf bifurcation ($\epsilon\,\mathrm{Le}^2<1$) from the region where the first primary bifurcation is a stationary one ($\epsilon\,\mathrm{Le}^2>1$). For $\varphi=+90°$ the motionless solution is infinitely linearly stable.

For some gas mixtures the Lewis number could be lower than one. In this situation, the regions of Hopf bifurcations and stationary bifurcations are separated by a curve depending not only on Le and ϵ but also on A and φ.

Some numerical investigations are carried out for a square cavity. The onset of motion is observed at the predicted Rayleigh number obtained by the linear theory. These nonlinear numerical simulations show the existence of multiple subcritical solutions. This linear analysis has to be completed by a nonlinear study to draw complete bifurcation diagrams for different sets of nondimensional parameters. The continuation method will be useful to follow the branch of solution (stable or unstable) created at the primary bifurcation points defined in this study.

ACKNOWLEDGMENTS

The authors gratefully acknowledge the C.N.U.S.C. (National center of computation, Montpellier, France) for its financial support and Dr. A. Bergeon for helpful discussions.

[1]M. A. Combarnous and S. A. Bories, ''Hydrothermal convection in saturated porous media,'' Adv. Hydrosci. **10**, 231 (1975).
[2]P. Cheng, ''Heat transfer in geothermal systems,'' Adv. Heat Transfer **14**, 1 (1978).
[3]O. Trevisan and A. Bejan, ''Combined heat and mass transfer by natural convection in porous medium,'' Adv. Heat Transfer **20**, 315 (1990).
[4]D. A. Nield and A. Bejan, *Convection in Porous Medium* (Springer, Berlin, 1992).
[5]R. W. Griffith, ''Layered double-diffusive convection in porous media,'' J. Fluid Mech. **102**, 221 (1981).
[6]P. T. Imhoff and T. Green, ''Experimental investigation of double-

diffusive groundwater fingers,'' J. Fluid Mech. **188**, 363 (1988).
[7]B. T. Murray and C. F. Chen, ''Double-diffusive convection in a porous medium,'' J. Fluid Mech. **201**, 147 (1989).
[8]O. Trevisan and A. Bejan, ''Mass and heat transfer by natural convection in a vertical slot filled with porous medium,'' Int. J. Heat Mass Transf. **29**, 403 (1986).
[9]F. Alavyoon, ''On natural convection in vertical porous enclosures due to prescribed fluxes of heat and mass at the vertical boundaries,'' Int. J. Heat Mass Transf. **36**, 2479 (1993).
[10]F. Alavyoon, Y. Masuda, and S. Kimura, ''On natural convection in vertical porous enclosures due to opposing fluxes of heat and mass prescribed at the vertical walls,'' Int. J. Heat Mass Transf. **37**, 195 (1994).
[11]M. Mamou, P. Vasseur, E. Bilgen, and D. Gobin, ''Double-diffusive convection in an inclined slot filled with porous medium,'' Eur. J. Mech. B/Fluids **14**, 629 (1995).
[12]M. Mamou, P. Vasseur, and E. Bilgen, ''Multiple solutions for double-diffusive convection in a vertical porous enclosure,'' Int. J. Heat Mass Transf. **38**, 1787 (1995).
[13]D. A. Nield, ''Onset of thermohaline convection in a porous medium,'' Water Resour. Res. **4**, 553 (1968).
[14]D. A. Nield, D. M. Manole, and J. L. Lage, ''Convection induced by inclined thermal and solutal gradients in a shallow horizontal layer of a porous medium,'' J. Fluid Mech. **257**, 559 (1981).
[15]J. W. Taunton, E. N. Lightfoot, and T. Green, ''Thermohaline instability and salt fingers in a porous medium,'' Phys. Fluids **15**, 748 (1972).
[16]O. V. Trevisan and A. Bejan, ''Mass and heat transfer by high Rayleigh number convection in a porous medium heated from below,'' Int. J. Heat Mass Transf. **30**, 2341 (1987).
[17]N. Rudraiah, P. K. Srimani, and R. Friedrich, ''Finite amplitude convection in a two-component fluid saturated porous layer,'' Int. J. Heat Mass Transf. **25**, 715 (1982).
[18]H. R. Brand, P. C. Hohenberg, and V. Steinberg, ''Amplitude equation near a polycritical point for the convective instability of a binary fluid mixture in a porous medium,'' Phys. Rev. A **27**, 591 (1983).
[19]O. V. Trevisan and A. Bejan, ''Natural convection with combined heat and mass transfer buoyancy effects in a porous medium,'' Int. J. Heat Mass Transf. **8**, 1597 (1985).
[20]M. C. Charrier-Mojtabi, M. Karimi-Fard, M. Azaïez, and A. Mojtabi, ''Onset of a double-diffusive convective regime in a rectangular porous cavity,'' J. Porous Media **1**, 104 (1998).
[21]D. Gobin and R. Bennacer, ''Double diffusion in a vertical fluid layer: Onset of the convective regime,'' Phys. Fluids **6**, 59 (1994).
[22]K. Ghorayeb and A. Mojtabi, ''Double-diffusive convection in vertical rectangular cavity,'' Phys. Fluids **9**, 2339 (1997).
[23]S. Xin, P. Le Quéré, and L. Tuckerman, ''Bifurcation analysis of double-diffusive convection with opposing horizontal thermal and solutal gradients,'' Phys. Fluids **10**, 850 (1998).
[24]R. G. Drazin and W. H. Reid, *Hydrodynamic Stability* (Cambridge University Press, Cambridge, 1981).
[25]B. Straughan, *The Energy Method, Stability and Nonlinear Convection* (Springer, Berlin, 1992), pp. 217–224.
[26]E. R. Lapwood, ''Convection of fluid in a porous medium,'' Proc. Cambridge Philos. Soc. **44**, 508 (1948).
[27]J. D. Crawford and E. Knobloch, ''Symmetry and symmetry-breaking bifurcations in fluid dynamics,'' Annu. Rev. Fluid Mech. **23**, 341 (1991).
[28]S. V. Patankar, *Numerical Heat Transfer and Fluid Flow* (McGraw–Hill, New York, 1980).
[29]B. Goyeau, J. P. Songbe, and D. Gobin, ''Numerical study of double-diffusive natural convection in a porous cavity using the Darcy–Brinkman formulation,'' Int. J. Heat Mass Transf. **39**, 1363 (1996).